Voltage Control Strategies for Solid Oxide Fuel Cell Energy System Connected to Complex Power Grids Using Dynamic State Estimation and STATCOM

Shenglong Yu, *Student Member, IEEE*, Tyrone Fernando, *Senior Member, IEEE*,
Tat Kei Chau, *Student Member, IEEE*, and Herbert Ho-Ching Iu, *Senior Member, IEEE*

***Abstract*—In this paper, a novel Dynamic State Estimation–current feedback with STATCOM control scheme is proposed for the mitigation of voltage fluctuation of Solid Oxide Fuel Cell (SOFC) power station connected to the complex power grids during electrical faults. The proposed control scheme is compared to two existing control strategies and shows its superiority in alleviating voltage flickers and deviations as well as protecting the internal membranes of the fuel cells. Since SOFC internal dynamic states are able to closely reflect the transience and dynamic behavior of SOFC, using them in controller designs can generate better regulations of the state-related internal voltage of SOFC than other methods. STATCOM is also utilized in this study to mitigate the voltage oscillations induced by unavoidable voltage fluctuations during electrical faults. The power system with proposed control strategy is proven to be stable through linear analysis. The acquisition of the useful internal dynamic states is realized using unscented Kalman filter algorithm based state estimator. The success of incorporating estimated states into the development of control strategies is conducive to the designs and implementations of new control schemes for power systems and also the applications of interdisciplinary control theories.**

***Index Terms*—Dynamic state estimation, fluctuation mitigation, SOFC, STATCOM, voltage control.**

I. Introduction

FUEL CELLS (FCS) are considered a type of clean energy source due to their zero emission and high fuel efficiency. Although finding more affordable catalysts and economical methodologies to produce huge quantities of hydrogen still challenge researchers and manufacturers, the efforts of exploiting and perfecting fuel cell energy systems have never ceased. Fuel cells have an extremely wide spectrum of domestic and industrial applications. Fig. 1 summarizes fuel cell applications[1], [2]. It can be clearly seen that low temperature Proton Exchange Membrane FC (PEMFC) and high temperature Solid Oxide FC (SOFC) have the widest variety of applications. Recent research work has focused on SOFC and PEMFC mathematical modeling, dynamic state estimation and control strategy developments. In [3], an application-oriented mathematical model of SOFC has been developed and verified in MATLAB SIMULINK, as well as with physical electric circuits, and has been widely adopted in research papers thereafter. The study of dynamic behavior and internal states of SOFC have been performed in [4], where SOFC power plant is connected to a complex power grid and a decentralized dynamic state estimator is designed and implemented to obtain the otherwise unaccessible dynamic states. Similarly, researchers of [5] have devised an adaptive state estimation methodology to track the internal dynamic states of PEMFC.

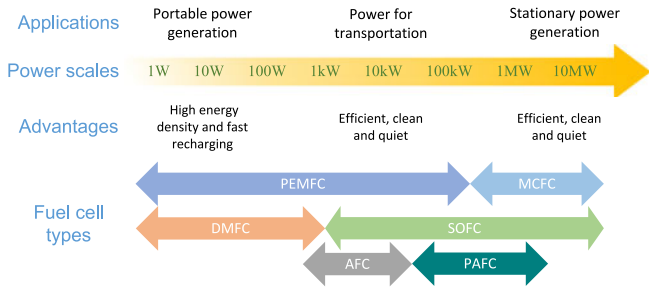

Fig. 1. Fuel cell applications.

On the control front, in [6] a simplified sliding mode control scheme is proposed to maintain the internal gas pressures in PEMFC to dwell in a safe region so as to protect the precious membrane, and in [7] a novel quasi-2D tubular anode-supported SOFC modeling approach is proposed for real-time control implementations. Optimal charging rate control strategy of plug-in electric vehicles (PEVs) is proposed in [8] to reduce the stress of power systems caused by poorly allocated multiple simultaneous charging terminals. In [9], the authors proposed a control scheme using the output DC current of the SOFC or the current magnitude of the AC load to modulate the hydrogen-flow rate of the SOFC connected to a multi-type power generation system. In [3], a constant fuel utilization control strategy has been proposed and implemented to an infinite-bus connected SOFC in order to make best use of the fuel. An analysis of a grid-connected fuel cell during faulty situations is performed in [10], where different faults are implemented and analyzed. In [11], an SOFC-ultracapacitor hybrid system is investigated, where the fuel starvation problem is prevented by regulating the fuel cell currents. Nevertheless, there has been no reported work on

Manuscript received April 27, 2016; revised July 28, 2016 and September 6, 2016; accepted October 1, 2016. Date of publication October 4, 2016; date of current version June 16, 2017. Paper no. TPWRS-00655-2016.

The authors are with the School of Electrical, Electronic and Computer Engineering, University of Western Australia, Crawley, WA 6009, Australia (e-mail: s.yu@ieee.org; tyrone.fernando@uwa.edu.au; tk.chau@ieee.org; herbert.iu@uwa.edu.au).

Color versions of one or more of the figures in this paper are available online at http://ieeexplore.ieee.org.

Digital Object Identifier 10.1109/TPWRS.2016.2615075

stability enhancement of SOFC power plant connected to complex power systems. With the growing popularity of SOFC power plants and the tendency of using SOFC as stationary power supply systems, it is necessary to investigate the dynamic behavior of SOFC connected to power networks with realistic configurations and speculations. Furthermore, the existing stability enhancement strategies mainly make use of the DC current of SOFC or fuel utilization rate. However, the protection of membranes and voltage stability enhancement strategies have not been investigated.

In this study, an SOFC power plant is connected to an IEEE standard complex power system and its dynamical behavior during electrical faults is studied and presented. In order to mitigate the voltage fluctuation and deviation and the damage that may be caused to the internal structure of fuel cells during faults, three control methods are proposed and presented. The newly proposed DSE-current dual feedback strategy demonstrates better control performances than existing ones with less voltage oscillations, a more favorable voltage level, and a faster settling time. The proposed DSE-current dual feedback scheme is also capable of regulating the pressures of reactant gases inside the SOFC channels, which produces a better protection for the internal membranes of SOFC units. STATCOM is also incorporated so as to further improve the voltage regulation performances. The control strategy for SOFC is to regulate the DC voltage output voltage in order to control the AC bus voltage, to which it connects. Moreover, a STATCOM is provided to further mitigate the fluctuations in AC bus voltage during electrical faults. SOFC control strategy and STATCOM are linked in a complementary fashion to stabilize and maintain the AC bus voltage during electrical faults. The proposed combined DSE-current dual feedback and STATCOM control strategy issues the best control results among all control schemes. The dynamic state estimator is designed using unscented Kalman filter algorithm [4]. The proposed control strategies theoretically achieve the realization of using electrical signals and power electronic devices to regulate chemical energy systems. Linear analysis shows that the power system with proposed control strategy retains overall system stability.

STATCOM is a shunt device of Flexible AC Transmission Systems (FACTS) family that uses electronic devices to control power flow and improve transient stability on power grids. STATCOM is capable of regulating bus voltages by providing or absorbing reactive power to or from bus-bars [12]. In the field of power system analysis and stability enhancement, this device has been reported to be used to alleviate fluctuations in power systems and thus improve power quality and stability in recent published academic papers [13], [14]. The former examines the application of STATCOM and battery energy storage to enhance the transient stability of large-scale multi-machine power systems, while the latter proposes an adaptive power oscillation damping (POD) controller for STATCOM equipped with energy storage in order to increase the damping effect at frequencies of interests. The utilization of STATCOM in this paper is aimed to further enhance the stability of SOFC terminal voltage.

The rest of the paper is organized as follows. In Section II, the mathematical model of electrochemical and thermochemical aspects of SOFC is concisely presented, which is followed by its mathematical connection to a complex power system. Different control strategies are proposed in subsections of Section III, all of which are then implemented in the case study with their simulation results compared and discussed. The paper concludes in Section IV.

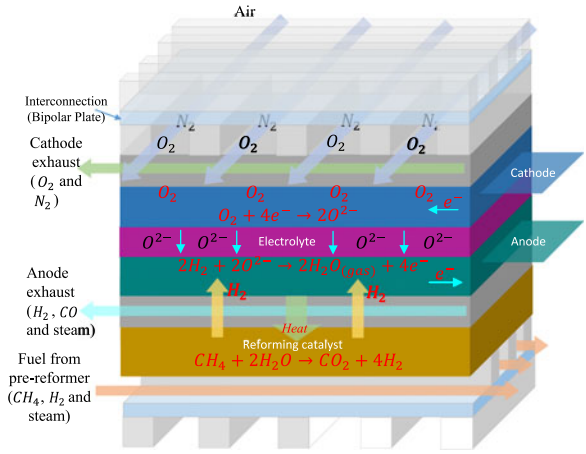

Fig. 2. Single solid oxide fuel cell schematic.

II. SOFC Mathematical Model and System Configuration

A. Stand-Alone SOFC Mathematical Model

SOFC uses an oxide ion-conducting ceramic material as the electrolyte. The most effective electrolytes are built on zirconia with a small percentage of yttria and the former material becomes an O^{2-} conductor above 800 °C. The state-of-the-art SOFCs operate between 800 °C and 1100 °C. Internal reforming happens in SOFC, where the entry fuel (CH_4) is 'reformed' into hydrogen, which transfers to anode and participates in the chemical reaction. Mixed gas containing hydrogen and carbon monoxide after the reforming process exits SOFC as part of the anode exhaust. High operating temperatures make precious metal electro-catalysts unnecessary in SOFC. For more details about internal reforming of SOFC and additional information in regard to its electrochemical aspect, see [1]. The schematic of an SOFC unit is shown in Fig. 2, and its mathematical derivations are briefly presented in Appendix A. Important dynamical equations of an SOFC are shown as follows. With SOFC states being $x_{\text{fc}} = [P^{\text{ch}}_{H_2}, P^{\text{ch}}_{H_2O}, P^{\text{ch}}_{O_2}, \eta_{\text{edl}}, T, T_{\text{ast}}, T^{\text{ann}}_{\text{air}}, T_{\text{fuel}}, T^{\text{ast}}_{\text{air}}]^T$, the state space equations of SOFC can be formed with dynamic equations (26), (27), (28), (38), (40), (41), (42), (43) and (44). This state space equation is shown as follows,

$$\dot{x}_{\text{fc}} = \begin{bmatrix} \dot{P}^{\text{ch}}_{H_2} \\ \dot{P}^{\text{ch}}_{H_2O} \\ \dot{P}^{\text{ch}}_{O_2} \\ \dot{\eta}_{\text{edl}} \\ \dot{T} \\ \dot{T}_{\text{ast}} \\ \dot{T}^{\text{ann}}_{\text{air}} \\ \dot{T}_{\text{fuel}} \\ \dot{T}^{\text{ast}}_{\text{air}} \end{bmatrix} = \begin{bmatrix} -\frac{JRT}{2\mathcal{F}\mathcal{V}_a} + \frac{2M^v_a RT(P^{\text{in}}_{H_2} - P^{\text{ch}}_{H_2})}{\mathcal{V}_a P_a} \\ -\frac{JRT}{4\mathcal{F}\mathcal{V}_c} + \frac{2M^v_c RT(P^{\text{in}}_{O_2} - P^{\text{ch}}_{O_2})}{\mathcal{V}_c P_c} \\ -\frac{JRT}{4\mathcal{F}\mathcal{V}_c} + \frac{2M^v_c RT(P^{\text{in}}_{O_2} - P^{\text{ch}}_{O_2})}{\mathcal{V}_c P_c} \\ \frac{1}{C_{\text{eq}}}\left(J - \frac{\eta_{\text{edl}}}{R_{\text{act}} + R_{\text{conc}}}\right) \\ \frac{Q_{\text{rad}} + Q^{\text{ast}_{\text{outer}}}_{\text{conv}} - Q^{\text{ast}_{\text{inner}}}_{\text{conv}} - Q^{\text{air}_{\text{ast}}}_{\text{flow}}}{m_{\text{ast}}\mathcal{C}_{\text{ast}}} \\ \frac{Q^{\text{ann}}_{\text{conv}}}{m^{\text{ann}}_{\text{air}}\mathcal{C}_{\text{air}}} \\ \frac{Q^{\text{fuel}}_{\text{conv}}}{m_{\text{fuel}}\mathcal{C}_{\text{fuel}}} \\ \frac{Q^{\text{ast}_{\text{inner}}}_{\text{conv}}}{m_{\text{air}}\mathcal{C}_{\text{air}}} \end{bmatrix}. \quad (1)$$

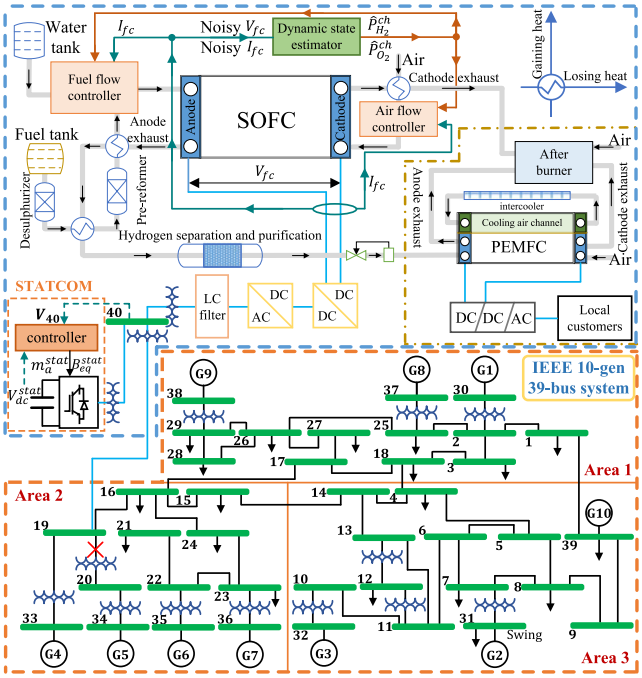

Fig. 3. SOFC power plant connected to IEEE standard 39-bus test system with estimation and control schemes.

This state space equation set will be reformatted later to suit the implementation of state estimation.

B. System Configuration

Fig. 3 illustrates the configuration of the test power system in question. The upper half of the figure is a simplified SOFC–PEMFC hybrid system. The rationale behind this design is that directly burning the highly concentrated hydrogen that comes out of the anode of SOFC has been considered a great waste of energy due to the high cost of acquiring purified hydrogen. In the hybrid system, hydrogen existing in SOFC anode exhaust is filtered and purified, which is then fed to the anode inlet of PEMFC through a series of further reactions, as shown in Fig. 3. This establishment has been proven to able to minimize heat and exergy losses. For more information about the SOFC–PEMFC hybrid system, see [1] and [15]. In this study, the inclusion of PEMFC in the yellow region in Fig. 3 is to reduce fuel wastes, which only provides power for local customers and does not share any power consumption from the main grid. A widely used validated PEMFC model can be found in [16].

The output DC voltage of SOFC power station passes a DC-DC boost converter and a DC-AC inverter and connects to bus 40 through a transformer. Bus 40 is then connected to bus 19 of the IEEE standard 3-area, 10-generator, 39-bus hybrid power system, which is shown in the lower half of Fig. 3, whose configuration is adopted from[17] where detailed mathematical modeling procedures are presented. The detailed mathematical model of SOFC and its derivation can be found in [3]. Assuming individual fuel cells can be lumped together to form a fuel cell stack and ignoring manufacturing dissimilarities and aging effects, the total fuel cells output voltage V_{fc} is linearly proportional to the output voltage of a single fuel cell V_{cell} [3], [10], [18]. With given connections, SOFC's mathematical model is re-addressed as follows. The dynamic state vector of SOFC is $x_{\text{fc}} = [P^{\text{ch}}_{H_2}, P^{\text{ch}}_{H_2O}, P^{\text{ch}}_{O_2}, \eta_{\text{edl}}, T, T_{\text{ast}}, T^{\text{ann}}_{\text{air}}, T_{\text{fuel}}, T^{\text{ast}}_{\text{air}}]^T$, input vector from the power system is $u_{\text{fc}} = [V_{40}, \theta_{40}, I_{40}, \gamma_{40}]^T$, where $V_{40}\angle\theta_{40}$ and $I_{40}\angle\gamma_{40}$ are the voltage of bus 40 and the current injected to bus 40, and the output is $y_{\text{fc}} = V_{\text{fc}}$. The terminal voltage and current are affected not only by the intrinsic characteristics of SOFC power plant, but also by the dynamical behavior of the complex power system to which SOFC is connected. Considering the dynamical equations, the general form of SOFC can be written as [4],

$$\begin{aligned} \dot{x}_{\text{fc}} &= f_{\text{fc}}(x_{\text{fc}}, u_{\text{fc}}), \\ 0 &= g_{\text{fc}}(x_{\text{fc}}, u_{\text{fc}}), \\ y_{\text{fc}} &= h_{\text{fc}}(x_{\text{fc}}, u_{\text{fc}}), \end{aligned} \tag{2}$$

where $f_{\text{fc}}(\cdot)$ and $h_{\text{fc}}(\cdot)$ are the fuel cell state and output functions derived from Section II and $g_{\text{fc}}(\cdot)$ represents the algebraic equations derived based on KVL that describe the connection of the SOFC power plant to the bus bar. The 10 synchronous generators are in three separate areas, and in each area one generator has a type I, IEEE ST1A AVR with PSS excitation system and all other generators are equipped with excitation systems of type II, IEEE DC1A AVR without PSS. Speed-governing systems of the 10 generators are categorized into two main types: (i) mechanical-hydraulic and (ii) electro-hydraulic with/without steam feedback. Hydro and steam turbines are also considered in the generation units. All the implemented steam turbines are tandem-compound, double or single reheat type. For generator and speed-governing equations, see reference [17]. The dynamic behavior of synchronous generators connected to SOFC power plant is studied in [4]. For the purpose of this study, this aspect is omitted. All the equations can be expressed mathematically in the following compact form [4],

$$\begin{aligned} \dot{\tilde{x}}_i &= \tilde{f}_i(\tilde{x}_i, \tilde{u}_i), \\ 0 &= \tilde{g}_i(\tilde{x}_i, \tilde{u}_i), \\ \tilde{y}_i &= \tilde{h}_i(\tilde{x}_i, \tilde{u}_i), \end{aligned} \tag{3}$$

for $i \in \{1, \ldots, 10\}$, where state vector $\tilde{x}_i$ consists of dynamic states of each generator, $\tilde{u}_i$ is the input vector, $\tilde{y}_i$ is the output vector, $\tilde{f}_i(\cdot)$ and $\tilde{h}_i(\cdot)$ are state and output functions derived from the mathematical models of each generator and $\tilde{g}_i(\cdot)$ is a set of algebraic equations that relate each generator stator to the bus voltage. The above equation compact form, together with the following power balance equation describes the whole power system [17],

$$P_{Ll} + jQ_{Ll} + V_l I_l e^{j(\theta_l - \gamma_l)} - \sum_{r=1}^{40} v_l v_r Y_{lr} e^{j(\theta_l - \theta_r - \phi_{lr})} = 0, \tag{4}$$

where $Y_{lr}\angle\phi_{lr}$ is the admittance of the transmission line connecting bus l and r, P_{Ll} and Q_{Ll} are active power and reactive power consumed by the loads connected to busbar l at time t. The above discussion and the compact format facilitate the implementation of the UKF in order to acquire the internal dynamic states. The detailed explanation, implementation and procedures

of using UKF filtering algorithm to obtain the internal dynamic states of SOFC has been reported in [4]. While other possible methods can also be utilized to acquire the internal dynamic states of SOFC, in this study, we make use of UKF algorithm to fulfill the task as it has been proven to be capable of providing accurate state estimates in [4], [19].

III. SOFC Control Strategies and Simulation Results

In this section, four control strategies are presented for the mitigation of the voltage fluctuations and deviations during electrical faults and the newly proposed DSE-based control together with STATCOM demonstrates the best flicker mitigation performance and fuel cell membrane protection. The motives behind the design of the control strategies are briefly presented as follows. In order to regulate the terminal voltage to settle to a lower value, we need to consider the components that contribute to the steady state voltage generated by a unit of the fuel cell. Based on equation (32), one can easily obtain the equation below,

$$\begin{aligned} V_{\text{cell}} &= E_{\text{nst}} - \eta_{\text{act}} + \eta_{\text{conc}} - \eta_{\text{ohm}} \\ &= E^0 + \frac{RT}{4\mathcal{F}} \ln\left(\frac{(P^{\text{ch}}_{H_2})^2 P^{\text{ch}}_{O_2}}{(P^{\text{ch}}_{H_2O})^2}\right) - \eta_{\text{act}} - \eta_{\text{ohm}} \\ &\quad - \frac{RT}{4\mathcal{F}} \ln\left(\frac{(P^{\text{ch}}_{H_2})^2 (P^{\text{eff}}_{H_2O})^2 P^{\text{ch}}_{O_2}}{(P^{\text{eff}}_{H_2})^2 (P^{\text{ch}}_{H_2O})^2 P^{\text{eff}}_{O_2}}\right) \\ &= E^0 - \eta_{\text{act}} - \eta_{\text{ohm}} + \frac{RT}{4\mathcal{F}} \ln\left(\frac{(P^{\text{eff}}_{H_2})^2 P^{\text{eff}}_{O_2}}{(P^{\text{ch}}_{H_2O})^2}\right), \end{aligned} \quad (5)$$

where standard potential E^o is a constant determined by the intrinsic characteristics of the fuel cells, and both activation and ohmic polarization voltage losses are functions of both temperature and current. According to equations (29), (30), (31), all effective partial pressures of gases are related to their partial pressures in the channels $P^{\text{ch}}_{H_2}$, $P^{\text{ch}}_{O_2}$, $P^{\text{ch}}_{H_2O}$ and the current density J. According to (26), (27) and (28), partial pressures in the channels are determined by the inlet gas molar flow rates and gas pressures at anode and cathode. It now follows that controlling the output voltage of a fuel cell (V_{cell}) is equivalent to controlling the input molar flow rate, electrical current, and input pressures of anode and cathode.

A. Constant Fuel Utilization Control

Fuel utilization ratio $\mathcal{R}_{FU}$ is defined as[2], [3],

$$\mathcal{R}_{FU} = \frac{M^v_{\text{consumedfuel}}}{M^v_{\text{inletfuel}}}, \quad (6)$$

where $M^v_{\text{inletfuel}}$ denotes the molar follow rate of the inlet fuel. Hence, for hydrogen fuel cells, the fuel utilization factor in equation (6) can be rewritten as,

$$\mathcal{R}_{H_2} = \frac{M^v_{\text{consumed}H_2}}{M^v_{\text{tot}H_2}} = \frac{I_{\text{fc}}}{2\mathcal{F}M^v_{\text{tot}H_2}}. \quad (7)$$

Therefore, the molar flow rate of hydrogen at anode is calculated as,

$$M^v_{H_2} = \frac{I_{\text{fc}}}{2\mathcal{F}\mathcal{R}_{H_2}}. \quad (8)$$

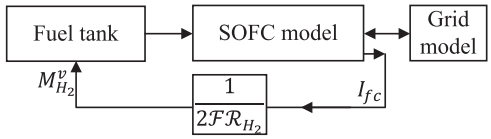

Fig. 4. Schematic representation of constant fuel utilization control.

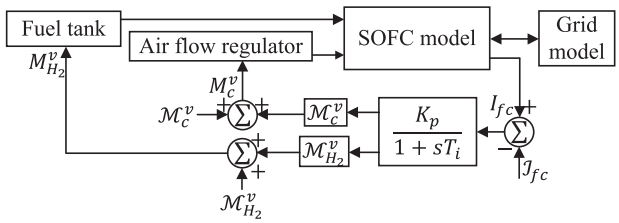

Fig. 5. Schematic representation of current feedback control.

Figure 4 illustrates the operating principle of this control strategy. The constant fuel utilization control is performed by adaptively controlling the inlet fuel flow rate to maintain a constant fuel utilization ratio. A 62% fuel utilization factor is adopted in this study[1], the rest of which goes to the PEMFC system for reuse. When the electrical fault occurs, the current fluctuates and thus the inlet flow rate of hydrogen at anode changes accordingly. More details about this control method can be found in [3]. This control scheme poses such shortcoming that as only the fuel utilization ratio is taken into consideration, the SOFC output voltage may still experience oscillations, and that the internal partial pressures may change significantly so that the membrane may be damaged.

B. Current Feedback Control

Current change during faults can partially reflect the demand of entry fuel and oxidant, and thus we propose a current feedback control strategy to regulate the input molar flow rate of hydrogen and oxygen by minimizing the difference between the fuel cell current I_{fc} and its nominal value $\mathcal{I}_{\text{fc}}$.

Fig. 5 demonstrates the schematic of this control method, based on which the differential equations describing the input molar flow rate of hydrogen and oxygen are derived as follows,

$$\begin{aligned} \frac{dM^v_{H_2}}{dt} &= \frac{1}{T_{i1}}\left(\mathcal{M}^v_{H_2}(1 + K_{p1}(I_{\text{fc}} - \mathcal{I}_{\text{fc}})) - M^v_{H_2}\right), \\ \frac{dM^v_c}{dt} &= \frac{1}{T_{i2}}\left(\mathcal{M}^v_c(1 + K_{p2}(I_{\text{fc}} - \mathcal{I}_{\text{fc}})) - M^v_c\right), \end{aligned} \quad (9)$$

where K_p and T_i are gain and time constant, respectively and $\mathcal{M}^v$ denotes nominal molar flow rate of specified gas species during initial steady state. The anode entry gas molar flow rate M^v_a is obtained as,

$$M^v_a = M^v_{H_2} + M^v_{H_2O}. \quad (10)$$

It can be noticed that during initial steady state, $dM^v_{H_2}/dt$ and dM^v_c/dt in (9) and (9) equal zero and $I_{\text{fc}} = \mathcal{I}_{\text{fc}}$, which render $M^v_{H_2} = \mathcal{M}^v_{H_2}$ and $M^v_{O_2} = \mathcal{M}^v_{O_2}$. This control scheme has such limitation that using electrical current as feedback signal may

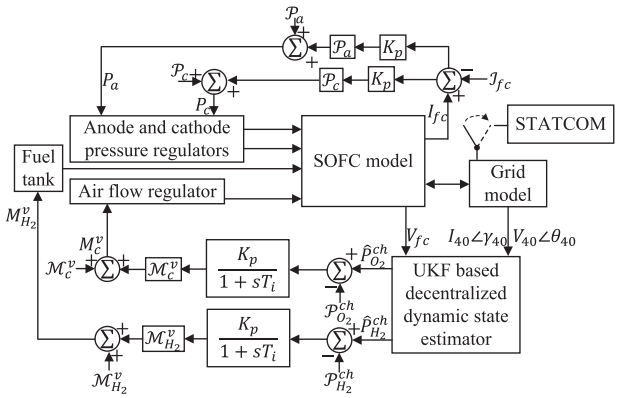

Fig. 6. Schematic representation of estimated gas pressures and current feedback control.

not be an adequate method to control the terms in equation (5) that relate to internal and effective partial pressures.

C. DSE–Current Dual Feedback Control

Internal partial pressures of gases in SOFC can reflect the performances of the fuel cell more precisely than merely observing the fuel usage ratio or current. For the purpose of this study, dynamical changes of internal partial pressures are used to construct the control signals that regulate the entry molar flow rates of hydrogen and air. The acquisition of the internal dynamic states is realized in a decentralized manner with the utilization of unscented Kalman filter algorithm and phasor measurement units. Estimated internal gas partial pressures $\hat{P}^{\text{ch}}_{H_2}$ and $\hat{P}^{\text{ch}}_{O_2}$, together with their nominal values during normal working condition are used to construct the control signal [6]. As both internal partial pressures and electrical current play important roles in regulating the output voltage of SOFC, current feedback is also used to control the pressures of anode and cathode inlet gases. Fig. 6 shows the schematic of this control strategy. The following differential equations are used to obtain their inlet molar flow rates,

$$\begin{aligned}\frac{dM^v_{H_2}}{dt} &= \frac{1}{T_{i3}}\left(\mathcal{M}^v_{H_2}(1+K_{p3}(\mathcal{P}^{\text{ch}}_{H_2}-\hat{P}^{\text{ch}}_{H_2}))-M^v_{H_2}\right),\\ \frac{dM^v_c}{dt} &= \frac{1}{T_{i4}}\left(\mathcal{M}^v_c(1+K_{p4}(\mathcal{P}^{\text{ch}}_{O_2}-\hat{P}^{\text{ch}}_{O_2}))-M^v_c\right),\end{aligned} \quad (11)$$

where $\mathcal{P}^{\text{ch}}$ denotes nominal partial pressure of the specified gas during normal operation condition. Equation (10) for calculating molar flow rate of gases at anode still holds. A set of proportional controllers are also incorporated to control the input gas pressures at anode and cathode with the following equations,

$$P_a = \mathcal{P}_a\left(1+K_{p5}(I_{\text{fc}}-\mathcal{I}_{\text{fc}})\right), \quad (12)$$

$$P_c = \mathcal{P}_c\left(1+K_{p6}(I_{\text{fc}}-\mathcal{I}_{\text{fc}})\right). \quad (13)$$

Maintaining the internal partial pressures of reactant gases has profound significance in not only alleviating the fluctuations of the output voltage and diminishing the voltage gap before and after fault, but also in protecting the precious membranes of fuel cells [6].

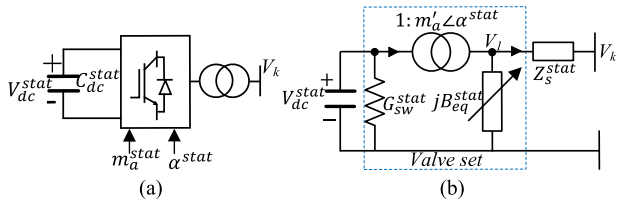

Fig. 7. (a) STATCOM schematic (b) VSC equivalent circuit.

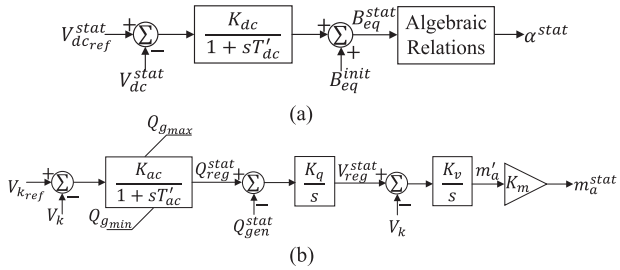

Fig. 8. (a) STATCOM DC-bus controller (b) STATCOM AC-bus controller.

D. STATCOM Control

With the aforementioned dual feedback controller, there may still be a number of unavoidable voltage fluctuations and voltage drops during electrical faults and thus STATCOM is used in this study to resolve this issue. The mathematical model of STATCOM in [20] is adopted in this study and briefly discussed as follows. The following power balance equation can be derived for the DC and AC parts of STATCOM,

$$P^{\text{stat}}_{\text{ac}} = P^{\text{stat}}_{\text{dc}} + P^{\text{stat}}_{\text{loss}}. \quad (14)$$

The configuration of STATCOM model, as shown in Fig. 7 consists of a two-level voltage source converter (VSC), which is physically built with a two-level converter using an array of PMW-driven self-commutating power electronic switches. It can be modeled as a load tap changing (LTC) transformer with its primary side connected to a small-rating capacitor bank and the secondary winding connected to the AC terminal through a series impedance [21]. As shown in Fig. 7(b), the model also includes a conductance $G^{\text{stat}}_{\text{sw}}$ to account for switching losses on the DC side and an equivalent shunt susceptance $B^{\text{stat}}_{\text{eq}}$ on the AC side, capable of providing and absorbing reactive power. Given the schematics for STATCOM and the VSC inside it, it has become clear that modulation index m^{stat}_a and phase angle α^{stat} are two crucial parameters that control the behavior of STATCOM, whose acquisition can be found in the block diagram in Fig. 8. From the block diagram, it is clear that controlling phase angle α^{stat} is equivalent to controlling susceptance $B^{\text{stat}}_{\text{eq}}$. The output m^{stat}_a and α^{stat} become the input of STATCOM to perform the voltage regulation, as shown in Fig. 7(a).

Fig. 8 shows the control blocks inside the STATCOM employed in this study, subscripts 'ref', 'max', 'min', 'gen', 'reg' denote the reference value, maximum value, minimum value, generated value and regulated value of specific variables, respectively, superscript 'init' denotes the initial value of equivalent susceptance, K and T' with different subscripts represent gains and time constants, and s is the Laplace variable. The

block 'algebraic relations' refer to (16). Generally speaking, the DC side generates the phase angle α^{stat} by minimizing the difference of DC voltage $V_{\text{dc}}^{\text{stat}}$ and its reference value, while the modulation index m_a^{stat} is generated at the AC end with the gap of bus voltage V_k and $V_{k_{ref}}$ being zeroed ($k = 40$ in this particular study). For more details about the STATCOM model and controller, refer to [20]. The STATCOM control block diagram can be translated into the following differential equations [20] and [22],

$$\frac{d}{dt}\begin{bmatrix} B_{\text{eq}}^{\text{stat}} \\ Q_{\text{reg}}^{\text{stat}} \\ V_{\text{reg}}^{\text{stat}} \\ m_a' \end{bmatrix} = \begin{bmatrix} T_{dc}'^{-1}\left(K_{dc}(V_{\text{dc}_{\text{ref}}}^{\text{stat}} - V_{\text{dc}}^{\text{stat}}) - B_{\text{eq}}^{\text{stat}}\right) \\ T_{ac}'^{\,-1}\left(K_{ac}(V_{k_{\text{ref}}} - V_k) - Q_{\text{reg}}^{\text{stat}}\right) \\ K_q(Q_{\text{reg}}^{\text{stat}} - Q_{\text{gen}}^{\text{stat}}) \\ K_v(V_{\text{reg}}^{\text{stat}} - V_{\text{gen}}^{\text{stat}}) \end{bmatrix}. \tag{15}$$

As the STATCOM power losses come from both series impedance Z_s^{stat} and switching loss conductance $G_{\text{sw}}^{\text{stat}}$, with equation (14) being valid, the following equations hold,

$$\begin{aligned} &P_{\text{ac}}^{\text{stat}} + m_a' V_k V_{\text{dc}}^{\text{stat}}\left(G_s^{\text{stat}}\cos(\theta_k - \alpha^{\text{stat}}) + B_s^{\text{stat}}\sin(\theta_k - \alpha^{\text{stat}})\right) \\ &\qquad - V_k^2 G_s^{\text{stat}} = 0, \\ &Q_{\text{ac}}^{\text{stat}} + m_a' V_k V_{\text{dc}}^{\text{stat}}\left(G_s^{\text{stat}}\sin(\theta_k - \alpha^{\text{stat}}) - B_s^{\text{stat}}\cos(\theta_k - \alpha^{\text{stat}})\right) \\ &\qquad + V_k^2 B_s^{\text{stat}} = 0, \\ &P_{\text{dc}}^{\text{stat}} + m_a' V_k V_{\text{dc}}^{\text{stat}}\left(G_s^{\text{stat}}\cos(\alpha^{\text{stat}} - \theta_k) + B_s^{\text{stat}}\sin(\alpha^{\text{stat}} - \theta_k)\right) \\ &\qquad - m_a'(G_s^{\text{stat}} + G_{\text{sw}}^{\text{stat}})(V_{\text{dc}}^{\text{stat}})^2 = 0, \\ &Q_{\text{dc}}^{\text{stat}} + m_a' V_k V_{\text{dc}}^{\text{stat}}\left(G_s^{\text{stat}}\sin(\alpha^{\text{stat}} - \theta_k) - B_s^{\text{stat}}\cos(\alpha^{\text{stat}} - \theta_k)\right) \\ &\qquad + m_a'(B_s^{\text{stat}} + B_{\text{eq}}^{\text{stat}})(V_{\text{dc}}^{\text{stat}})^2 = 0, \end{aligned} \tag{16}$$

where the conductance G_s^{stat} and susceptance B_s^{stat} are obtained by $G_s^{\text{stat}} + jB_s^{\text{stat}} = 1/Z_s^{\text{stat}}$. Differential-algebraic (15) and (16) are utilized for transient stability investigation in this study. STATCOM is used here to mitigate the residual voltage oscillations and regulate the voltage value by providing or absorbing proper amounts of reactive power to or from the bus bar. In this study, STATCOM is utilized with the proposed DSE-current feedback control scheme to alleviate the voltage oscillations and deviations during electrical faults.

E. Simulation Results

The simulation is conducted in MATLAB 2014b coding environment on a desktop computer with Intel Core i7-4790, 3.6 GHz CPU, 64-bit Windows7 operating system. The entire power system is simulated with MATLAB codes and simulation results are observed, acquired and analyzed using MATLAB built-in algebraic-differential-equation solvers in continuous time. The test system configuration is shown in Fig. 3. The simulation lasts for 20 seconds and the system is in steady state in the beginning. When $t = 1.2$ s, an electrical fault occurs and the transmission line between bus 19 and bus 20 is disconnected. Bus 19 is connected to bus 40, to which SOFC power station is connected, and thus any sudden change that occurs

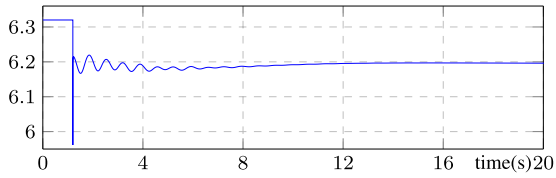

Fig. 9. Active power injected to bus 40 during the simulation.

TABLE I
MAJOR PARAMETERS

(1) Constant fuel utilization rate control							
$\mathcal{R}_{FU}$	10						
(2) Current feedback control							
T_{i1}	0.001	T_{i2}	0.001	K_{p1}	0.0358	K_{p2}	0.0358
(3) DSE-current feedback control							
T_{i3}	0.01	T_{i4}	0.01	K_{p3}	0.01	K_{p4}	0.05
K_{p5}	0.04	K_{p6}	0.035				
(4) ∗STATCOM (used with DSE-current feedback control)							
T_{dc}'	0.05	T_{ac}'	0.75	K_{dc}	40	K_{ac}	10
K_v	10	K_q	0.01				

∗STATCOM parameters are adopted and modified from [20].

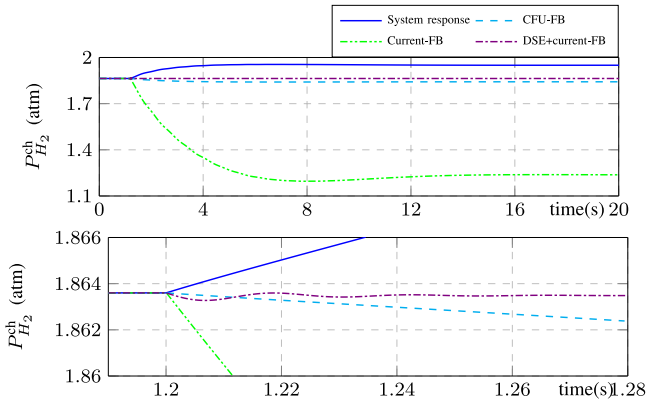

Fig. 10. Partial pressure of hydrogen in anode channel.

on bus 19 will affect the performances of SOFC. The choice of transmission line is aimed at best demonstrating the proposed control strategies during faults. The fault remains for the rest of the simulation. The aforementioned estimation and control schemes are implemented.

Fig. 9 shows the power variations during the simulation under no control situation. This figure is only to verify that less power is required during the fault and is within the capacity of SOFC power station. Table I demonstrates the parameters used in the three proposed control strategies. The rest of the parameters are thermodynamic constants and coefficients that can be found in [3], [23].

Figures 10 and 11 demonstrate the variations in hydrogen and oxygen partial pressures for the proposed constant fuel utilization (CFU) feedback (FB) control, current feedback control and combined DSE-current dual FB control. With their zoomed-in curves, one can observe their transience with different control strategies when the fault happens. As mentioned before, the DSE-current FB control strategy is aimed to maintain a small

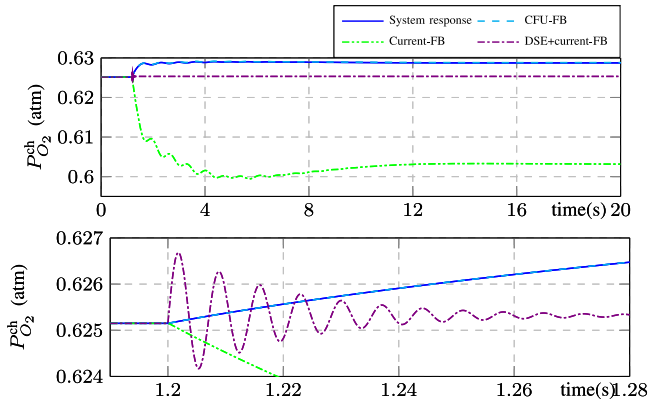

Fig. 11. Partial pressure of oxygen in cathode channel.

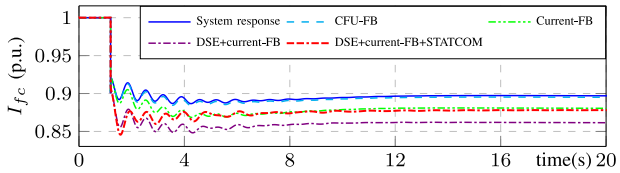

Fig. 12. Fuel cell current.

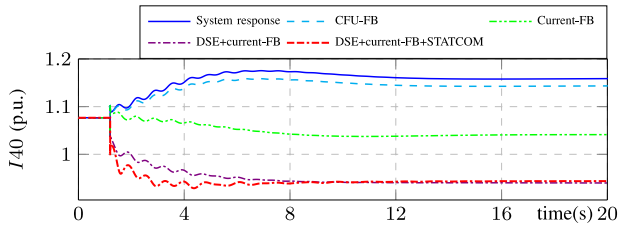

Fig. 13. Current injected to bus 40.

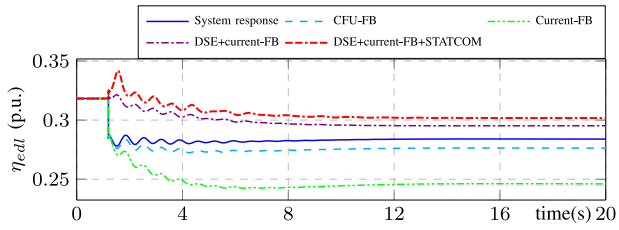

Fig. 14. Electric double layer voltage.

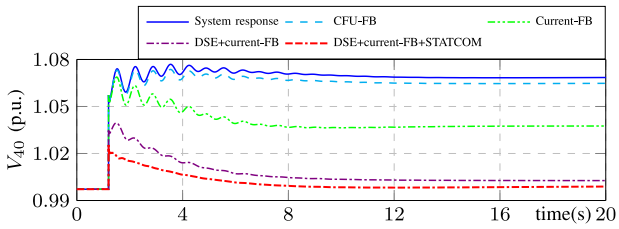

Fig. 15. Voltage of bus 40.

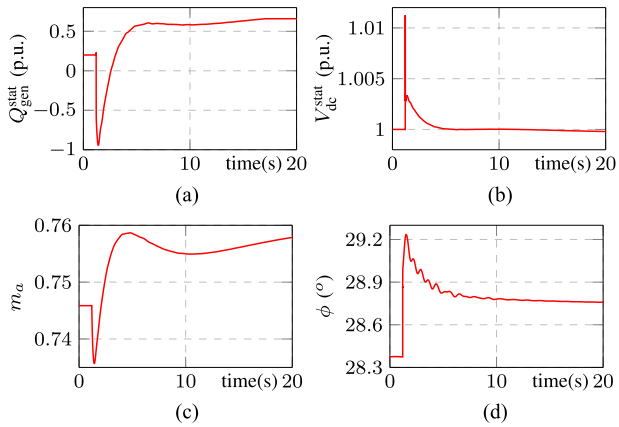

Fig. 16. (a) Generated reacitve power. (b) DC side voltage. (c) Modulation index. (d) Phase angle.

fluctuation in the internal partial pressures of hydrogen and oxygen and the figures have shown significantly better results in this aspect than other control schemes. To this end, the proposed DSE-current dual feedback control can provide the best protection for the membrane. We can also notice that the current FB control has issued the largest disturbance in the internal partial pressures, which may lead to damages of the physical structure inside fuel cells. Moreover, the CFU-FB control does not influence the partial pressure of oxygen but it is able to regulate the hydrogen partial pressure to a reasonable value. Figs. 12 and 13 show the regulations of fuel cell current and the current injected into bus 40 for the three control schemes and the newly proposed DES-current feedback control with STATCOM.

With the relationship between the electric double layer (EDL) voltage loss and the fuel cell current, Fig. 14 shows the EDL voltage drop for 4 control strategies. It can be noticed that current FB control has issued the lowest voltage drop in this type of polarization. Fig. 15 demonstrates the resultant terminal voltage of different controllers and it is obvious that the DSE-current dual FB controller produces the best result than other fuel cell input regulation control methods with a closest voltage level to the bus voltage under normal circumstances and fewest oscillations. However, the utilization of STATCOM issues an even more favorable voltage regulation result where STATCOM is capable of bringing the voltage during faulty operating condition almost to its regular level and alleviating the fluctuations in the DSE-current dual feedback control strategy.

On the STATCOM front, Fig. 16(a)∼(d) show the generated reactive $Q_{\text{gen}}^{\text{stat}}$, capacitor voltage $V_{\text{dc}}^{\text{stat}}$, the modulation index m_a^{stat} and the phase angle ϕ during the simulation. Together with the voltage variations and the control schematics, one can tell when the terminal voltage starts deviating, the modulation index and DC side voltage start changing, which lead to the variations in generated reactive power and the phase angle. Overall speaking, STATCOM manages to provide or absorb reactive power to or from the bus bar to try maintaining the bus voltage and DC side voltage at their nominal values.

It is noteworthy that the combined control strategy proposed in this study makes use of local current and voltage measurements to generate estimated internal dynamic states and also provide feedback signals. That is to say, the proposed method

operates in a decentralized manner, which makes the novel control strategy able to regulate SOFC power plants in any reasonable power network connections within the power capacity. The execution times for no-control, constant-fuel-utilization control, current-FB control and DSE-current dual FB control are respectively approximately 5.14 s, 5.18, 6.22 s and 11.3 s. These execution times may vary with different setting in MATLAB solvers, computer configurations and sampling times for UKF-based dynamic state estimator. The last factor has been reported in detail in [4].

F. Stability Assessment for Controller-Incorporated System

In order to assess the stability of the overall power system with control strategies, linear analysis is required. Due to the complexity of the power system in question, linearization process is only briefly discussed as follows. The overall STATCOM-integrated IEEE standard 39-bus, 10-generator power system can be written in the following compact form [17],

$$\frac{d}{dt}\mathbf{X} = F(\mathbf{X}, \mathbf{U}),$$
$$0 = G(\mathbf{X}, \mathbf{U}), \tag{17}$$
$$\mathbf{X} = \begin{bmatrix} \mathbf{x}_{\text{gen}} \\ \mathbf{x}_{\text{ctrl}} \\ \mathbf{x}_{\text{stat}} \end{bmatrix}, \quad \mathbf{U} = \begin{bmatrix} \mathbf{u}_{\text{gen}} \\ \mathbf{u}_{\text{ctrl}} \\ \mathbf{u}_{\text{stat}} \end{bmatrix}, \tag{18}$$

where $F(\cdot)$ and $G(\cdot)$ are respectively the state differential and algebraic functions of the system model, $\mathbf{X}$ is the system dynamic state vector consisting of generator state vector $\mathbf{x}_{\text{gen}}$ (including fuel cell state vector), control dynamic vector $\mathbf{x}_{\text{ctrl}}$, and STATCOM state vector $\mathbf{x}_{\text{stat}}$ and $\mathbf{U}$ is the system input vector, comprised of generator input vector $\mathbf{u}_{\text{gen}}$, control input vector $\mathbf{u}_{\text{ctrl}}$ and STATCOM input vector $\mathbf{u}_{\text{stat}}$. The following equations demonstrate the elements in state and input vectors for the aforementioned STATCOM-integrated power system,

$$\mathbf{x}_{\text{gen}} = [x_{\text{gen}_1}, x_{\text{gen}_2}, \ldots, x_{\text{gen}_{10}}, x_{\text{fc}}]^T, \tag{19}$$
$$\mathbf{x}_{\text{stat}} = [B_{\text{eq}}^{\text{stat}}, Q_{\text{reg}}^{\text{stat}}, V_{\text{reg}}^{\text{stat}}, m_a']^T, \tag{20}$$

and $\mathbf{x}_{\text{ctrl}}$ can be obtained based on different control strategies mentioned above. Detailed description of generator states $\mathbf{x}_{\text{gen}}$ can be found in [17]. The following equations illustrate the structure of the input vector,

$$\mathbf{u}_{\text{gen}} = [u_{\text{gen}_1}, u_{\text{gen}_2}, \cdots, u_{\text{gen}_{10}}, u_{\text{fc}}]^T, \tag{21}$$
$$\mathbf{u}_{\text{stat}} = [V_{\text{ref}}^{\text{stat}}, V_{dc_{\text{ref}}}^{\text{stat}}]^T, \tag{22}$$

and again $\mathbf{u}_{\text{ctrl}}$ varies according to different control strategies and is constituted by the reference values, for instance, $\mathcal{I}_{\text{fc}}$. Reference [24] provides detailed description of generator input vector $\mathbf{u}_{\text{gen}}$. As for the fuel cell input vector,

$$u_{\text{fc}} = [\mathcal{M}_{H_2}^v, \mathcal{M}_c^v, \mathcal{P}_a, \mathcal{P}_c]^T. \tag{23}$$

See [17] and [24] for specifics.

For small-signal stability analysis of the state space model, the following linearized system equation can be obtained,

$$\Delta\dot{\mathbf{X}} = A\Delta\mathbf{X} + B\Delta\mathbf{U}, \tag{24}$$

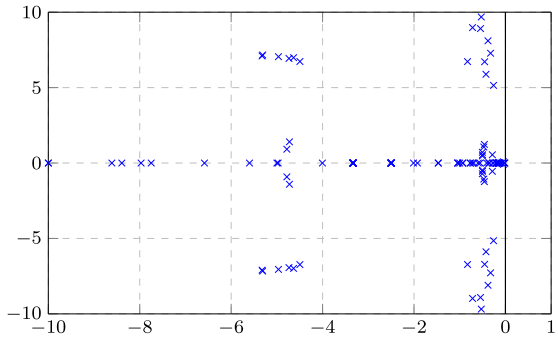

Fig. 17. System eigenvalue plot with DSE-current-FB-STATCOM method.

where A and B are coefficients of the linearized system. For detailed steps and derivations of linearizing nonlinear power systems, refer to [24].

After arduous mathematical procedures, a 152×152 system matrix A is obtained for the SOFC-connected power system with DSE-current-FB-STATCOM control method, equipped with control parameters shown in Table I. The system eigenvalue plot on the complex plane is shown in Fig. 17, where we can easily see that all the eigenvalues are on the open left half plane, hence system stability proven. Note that only a sub-part of the complex plane is shown for easy observation, and there are no positive-real-part eigenvalues found in this simulation study.

IV. Conclusion

In this paper, a dynamic state estimates-current dual feedback control strategy is proposed to mitigate the voltage oscillations and deviations during electrical faults, which uses electrical control signals to perform chemical control. The DSE-current dual feedback control has demonstrated its superiority in controlling the output voltage during electrical faults as well as its capability of protecting the fuel cell membranes by maintaining the internal partial pressures of reactant gases. This method, however, may still not be adequate to best alleviate the fluctuations in AC bus voltages that inherently exist during faults. Therefore, a power electronics device STATCOM is implemented to further reduce the voltage oscillations and deviations, which together with the DSE-current feedback controller has proven to be able to generate the best AC bus voltage regulation result. The overall power system with proposed control strategy retains its stability, which is proven through system linear analysis. Future work may involve further investigations of the universality of such electrical-chemical control methodologies by applying them to different types of power sources and energy systems.

Appendix A
Derivation of SOFC State Equations

The equations relating to stand-alone SOFC presented in Section II are briefly derived as follows. Assuming ideal gases participate in the chemical reaction, the following equation can express the Nernst potential in an SOFC unit [2],

$$E_{\text{nst}} = E^0 + \frac{RT}{4\mathcal{F}} \ln\left(\frac{(P_{H_2}^{\text{ch}})^2 P_{O_2}^{\text{ch}}}{(P_{H_2O}^{\text{ch}})^2}\right), \tag{25}$$

where E^0 is the internal potential under standard temperature and pressure conditions [3], R and $\mathcal{F}$ are the ideal gas constant and Faraday's constant respectively, T is the operating temperature and $P^{\text{ch}}_{H_2}$, $P^{\text{ch}}_{O_2}$, $P^{\text{ch}}_{H_2O}$ denote the partial pressure of gases in the channels. Note that temperature T has a significant impact on fuel cell operations. Its acquisition will be discussed later in this section. Using Maxwell-Stefan diffusion equation with a series of mathematical manipulations [23], the differential equations of partial pressures in channels $P^{\text{ch}}_{H_2}$, $P^{\text{ch}}_{H_2O}$ and $P^{\text{ch}}_{O_2}$, are shown as follows [25],

$$\frac{dP^{\text{ch}}_{H_2}}{dt} = -\frac{JRT}{2\mathcal{F}\mathcal{V}_a} + \frac{2M^v_a RT(P^{\text{in}}_{H_2} - P^{\text{ch}}_{H_2})}{\mathcal{V}_a P_a}, \tag{26}$$

$$\frac{dP^{\text{ch}}_{H_2O}}{dt} = \frac{JRT}{2\mathcal{F}\mathcal{V}_a} + \frac{2M^v_a RT(P^{\text{in}}_{H_2O} - P^{\text{ch}}_{H_2O})}{\mathcal{V}_a P_a}, \tag{27}$$

$$\frac{dP^{\text{ch}}_{O_2}}{dt} = -\frac{JRT}{4\mathcal{F}\mathcal{V}_c} + \frac{2M^v_c RT(P^{\text{in}}_{O_2} - P^{\text{ch}}_{O_2})}{\mathcal{V}_c P_c}, \tag{28}$$

where J is the current density flowing through an SOFC unit, $\mathcal{V}_a$ and $\mathcal{V}_c$ denote the volumes of anode and cathode channels, respectively and M^v_a and M^v_c denote the molar flow rates at anode and cathode. Then the reversible potential E_{nst} can be acquired based on (25). The effective partial pressures of hydrogen and water vapor at the actual reaction site can be calculated as [3], [4],

$$P^{\text{eff}}_{H_2} = P^{\text{ch}}_{H_2} + \frac{dP^{\text{ch}}_{H_2}}{dx} D_{\text{ar}} = P^{\text{ch}}_{H_2} - \frac{JRTD_{\text{ar}}}{2\mathcal{F}\mathcal{D}_{H_2,H_2O}}, \tag{29}$$

$$P^{\text{eff}}_{H_2O} = P^{\text{ch}}_{H_2O} + \frac{dP^{\text{ch}}_{H_2O}}{dx} D_{\text{ar}} = P^{\text{ch}}_{H_2O} + \frac{JRTD_{\text{ar}}}{2\mathcal{F}\mathcal{D}_{H_2O,H_2}}, \tag{30}$$

$$P^{\text{eff}}_{O_2} = P^{\text{ch}}_{O_2} \exp\left(\frac{RTJD_{\text{cr}}}{4\mathcal{F}P^{\text{ch}}_c \mathcal{D}_{O_2,N_2}}\right) + P^{\text{ch}}_c \left(1 - \exp\left(\frac{RTJD_{\text{cr}}}{4\mathcal{F}P^{\text{ch}}_c \mathcal{D}_{O_2,N_2}}\right)\right), \tag{31}$$

where D_{ar} and D_{cr} are the distances from anode and cathode surface to the reaction site respectively.

Due to several types of irreversible voltage losses inside SOFC, the actual voltage of fuel cell becomes lower than the Nernst potential [2]. The following equation describes the output voltage of an SOFC unit (V_{cell}),

$$V_{\text{cell}} = E_{\text{nst}} - \eta_{\text{act}} - \eta_{\text{ohm}} - \eta_{\text{conc}}, \tag{32}$$

where η_{act}, η_{ohm} and η_{conc} denote voltage drops of activation polarization, ohmic polarization and concentration polarization respectively, the first two of which are functions of both current density and SOFC operating temperature, while the voltage drop from concentration polarization is a function of partial pressures of gases in the channels $P^{\text{ch}}_{H_2}$, $P^{\text{ch}}_{H_2O}$, $P^{\text{ch}}_{O_2}$ and at the reaction site $P^{\text{eff}}_{H_2}$, $P^{\text{eff}}_{H_2O}$, $P^{\text{eff}}_{O_2}$. Butler-Volmer equation is used to express the activation polarization as follows,

$$J = J_0 \left(\exp\left(\beta n_e \frac{\mathcal{F}\eta_{\text{act}}}{RT}\right) - \exp\left(-(1-\beta) n_e \frac{\mathcal{F}\eta_{\text{act}}}{RT}\right)\right), \tag{33}$$

where J_0 is the exchange current density, n_e is the number of electrons and β is ion transfer coefficient. Under high-activation polarization, Tafel equation can be derived for the calculation of activation polarization voltage loss, which is shown as follows,

$$\eta_{\text{act}} = \frac{RT}{n_e\beta\mathcal{F}}\ln(J) - \frac{RT}{n_e\beta\mathcal{F}}\ln(J_0). \tag{34}$$

It can be seen that activation polarization voltage is a function of fuel cell internal temperature and can be rewritten in the following form,

$$\eta_{\text{act}} = \eta_{\text{act0}} + \eta_{\text{act1}}, \tag{35}$$

where η_{act0} is a function of internal temperature, while η_{act1} depends on both temperature and current density. Voltage drop due to ohmic polarization can be simply expressed with

$$\eta_{\text{ohm}} = JR_{\text{eq}}, \tag{36}$$

where R_{eq} is the equivalent ionic resistance of fuel cell, a function of the operating temperature. Concentration polarization happens at both cathode and anode, and can be expressed using following equations,

$$\begin{aligned}\eta_{\text{conc}} &= \eta^{\text{an}}_{\text{conc}} + \eta^{\text{ca}}_{\text{conc}} \\ &= -\frac{RT}{2\mathcal{F}}\ln\left(\frac{P^{\text{ch}}_{H_2O}}{P^{\text{ch}}_{H_2}} \cdot \frac{P^{\text{eff}}_{H_2}}{P^{\text{eff}}_{H_2O}}\right) - \frac{RT}{4\mathcal{F}}\ln\left(\frac{P^{\text{eff}}_{O_2}}{P^{\text{ch}}_{O_2}}\right), \\ &= \frac{RT}{4\mathcal{F}}\ln\left(\left(\frac{P^{\text{ch}}_{H_2}}{P^{\text{eff}}_{H_2}} \cdot \frac{P^{\text{eff}}_{H_2O}}{P^{\text{ch}}_{H_2O}}\right)^2 \cdot \left(\frac{P^{\text{ch}}_{O_2}}{P^{\text{eff}}_{O_2}}\right)\right).\end{aligned} \tag{37}$$

With the simplified model of Electrical Double Layer (EDL) charging effect, the following equation holds[1], [3],

$$\frac{d\eta_{\text{edl}}}{dt} = \frac{1}{C_{\text{eq}}}\left(J - \frac{\eta_{\text{edl}}}{R_{\text{act}} + R_{\text{conc}}}\right), \tag{38}$$

where R_{act} and R_{conc} are the equivalent resistances of activation and concentration polarizations. Then the expression of fuel cell output voltage can be modified as [3],

$$V_{\text{cell}} = E_{\text{nst}} - \eta_{\text{edl}} - \eta_{\text{act0}} - \eta_{\text{ohm}}. \tag{39}$$

With (34)–(37), the output voltage of a fuel cell unit in equation (39) is obtainable given the operating temperature of SOFC.

Radiation, convection and mass flow are the three main ways heat transfer occurs in an SOFC unit. For detailed explanation and derivations of equations, see [2], [3], [23]. Temperature-related differential equations are listed as follows,

$$\frac{dT}{dt} = \frac{Q_{\text{gen}} - Q_{\text{out}}}{\mathcal{C}_{\text{cell}} m_{\text{cell}}}, \tag{40}$$

$$\frac{dT_{\text{ast}}}{dt} = \frac{Q_{\text{rad}} + Q^{\text{ast}_{\text{outer}}}_{\text{conv}} - Q^{\text{ast}_{\text{inner}}}_{\text{conv}} - Q^{\text{air}_{\text{ast}}}_{\text{flow}}}{m_{\text{ast}}\mathcal{C}_{\text{ast}}}, \tag{41}$$

$$\frac{dT^{\text{ann}}_{\text{air}}}{dt} = \frac{Q^{\text{ann}}_{\text{conv}}}{m^{\text{ann}}_{\text{air}}\mathcal{C}_{\text{air}}}, \tag{42}$$

$$\frac{dT_{\text{fuel}}}{dt} = \frac{Q^{\text{fuel}}_{\text{conv}}}{m_{\text{fuel}}\mathcal{C}_{\text{fuel}}}, \tag{43}$$

$$\frac{dT^{\text{ast}}_{\text{air}}}{dt} = \frac{Q^{\text{ast}_{\text{inner}}}_{\text{conv}}}{m_{\text{air}}\mathcal{C}_{\text{air}}}, \tag{44}$$

where Q with subscripts 'gen', 'out', 'rad', 'conv' and 'flow' stand for generated, output, radiative, convective and flowing heat, superscripts 'ann' represents annulus, and $\mathcal{C}$ and m denote the heat capacity and mass of specified gas or component of SOFC. For more explanations and derivations of thermodynamic aspects of SOFC, see [1], [3] and [4].

REFERENCES

[1] J. Larminie, A. Dicks, and M. S. McDonald, *Fuel Cell Systems Explained*, vol. 2. New York, NY, USA: Wiley, 2003.

[2] A. J. Appleby, *Fuel Cell Handbook*, 7th ed. EG&G Tech. Services Inc., U.S. Dept. Energy Office Fossil Energy, Washington, DC, USA, Nov. 2004.

[3] C. Wang and H. M. Nehrir, "A physically based dynamic model for solid oxide fuel cells," *IEEE Trans. Energy Convers.*, vol. 22, no. 4, pp. 887–897, Dec. 2007.

[4] S. Yu, T. Fernando, and H. H.-C. Iu, "Dynamic behavior study and state estimator design for solid oxide fuel cells in hybrid power systems," *IEEE Trans. Power Syst.*, to be published.

[5] R. Vepa, "Adaptive state estimation of a PEM fuel cell," *IEEE Trans. Energy Convers.*, vol. 27, no. 2, pp. 457–467, Jun. 2012.

[6] G. Park and Z. Gajic, "A simple sliding mode controller of a fifth-order nonlinear PEM fuel cell model," *IEEE Trans. Energy Convers.*, vol. 29, no. 1, pp. 65–71, Mar. 2014.

[7] F. Gao, M. G. Simoes, B. Blunier, and A. Miraoui, "Development of a quasi 2-D modeling of tubular solid-oxide fuel cell for real-time control," *IEEE Trans. Energy Convers.*, vol. 29, no. 1, pp. 9–19, Mar. 2014.

[8] Y. Xu, "Optimal distributed charging rate control of plug-in electric vehicles for demand management," *IEEE Trans. Power Syst.*, vol. 30, no. 3, pp. 1536–1545, May 2015.

[9] L. Wang and D.-J. Lee, "Load-tracking performance of an autonomous SOFC-based hybrid power generation/energy storage system," *IEEE Trans. Energy Convers.*, vol. 25, no. 1, pp. 128–139, Mar. 2010.

[10] E. M. Stewart, R. Tumilty, J. Fletcher, A. Lutz, G. Ault, and J. McDonald, "Analysis of a distributed grid-connected fuel cell during fault conditions," *IEEE Trans. Power Syst.*, vol. 25, no. 1, pp. 497–505, Feb. 2010.

[11] T. Allag and T. Das, "Robust control of solid oxide fuel cell ultracapacitor hybrid system," *IEEE Trans. Control Syst. Technol.*, vol. 20, no. 1, pp. 1–10, Feb. 2012.

[12] N. G. Hingorani and L. Gyugyi, *Understanding FACTS*. Piscataway, NJ, USA: IEEE Press, 2000.

[13] A. Kanchanaharuthai, V. Chankong, and K. A. Loparo, "Transient stability and voltage regulation in multimachine power systems vis-à-vis STATCOM and battery energy storage," *IEEE Trans. Power Syst.*, vol. 30, no. 5, pp. 2404–2416, Sep. 2015.

[14] M. Beza and M. Bongiorno, "An adaptive power oscillation damping controller by STATCOM with energy storage," *IEEE Trans. Power Syst.*, vol. 30, no. 1, pp. 484–493, Jan. 2015.

[15] A. Rabbani and M. Rokni, "Modeling and analysis of transport processes and efficiency of combined SOFC and PEMFC systems," *Energies*, vol. 7, no. 9, pp. 5502–5522, 2014.

[16] C. Wang, M. H. Nehrir, and S. R. Shaw, "Dynamic models and model validation for PEM fuel cells using electrical circuits," *IEEE Trans. Energy Convers.*, vol. 20, no. 2, pp. 442–451, Jul. 2005.

[17] T. Fernando, K. Emami, S. Yu, H. H.-C. Iu, and K. P. Wong, "A novel quasi-decentralized functional observer approach to LFC of interconnected power systems," *IEEE Trans. Power Syst.*, vol. 31, no. 4, pp. 3139–3151, Jul. 2016.

[18] C. Wang, M. Nehrir, and H. Gao, "Control of PEM fuel cell distributed generation systems," *IEEE Trans. Energy Convers.*, vol. 21, no. 2, pp. 586–595, Jun. 2006.

[19] A. K. Singh and B. C. Pal, "Decentralized dynamic state estimation in power systems using unscented transformation," *IEEE Trans. Power Syst.*, vol. 29, no. 2, pp. 794–804, Mar. 2014.

[20] L. M. Castro, E. Acha, and C. R. Fuerte-Esquivel, "A novel STATCOM model for dynamic power system simulations," *IEEE Trans. Power Syst.*, vol. 28, no. 3, pp. 3145–3154, Aug. 2013.

[21] C. A. Canizares, "Power flow and transient stability models of FACTS controllers for voltage and angle stability studies," in *Proc. IEEE Power Eng. Soc. Winter Meeting*, 2000, vol. 2, pp. 1447–1454.

[22] E. Acha and B. Kazemtabrizi, "A new STATCOM model for power flows using the Newton–Raphson method," *IEEE Trans. Power Syst.*, vol. 28, no. 3, pp. 2455–2465, Aug. 2013.

[23] M. Planck, *Treatise on Thermodynamics*. North Chelmsford, MA, USA: Courier Corp., 2013.

[24] P. W. Sauer, *Power System Dynamics and Stability*. Englewood Cliffs, NJ, USA: Prentice Hall, 1998.

[25] G. N. Hatsopoulos and J. H. Keenan, *Principles of General Thermodynamics*, vol. 398. New York, NY, USA: Wiley, 1965.

Shenglong Yu (S'15) received the Bachelor's degree (Hons.) in measurement and control technology and instrumentation from China University of Geosciences, Beijing, China, in 2011 and the Master's degree in electrical and electronic engineering with Distinction from the University of Western Australia, Crawley, WA, Australia, in 2014, where he is currently working toward the Ph.D. degree. His research interests are in renewable energy integration, power system analysis and control, smart grids, microgirds, load and renewable power forecasting, and dynamic state estimation algorithms.

Tyrone Fernando (M'95–SM'05) received the B.Eng. (Hons.) degree and the Doctor of Philosophy degree from the University of Melbourne, Parkville, VIC, Australia, in 1990 and 1996, respectively. In 1996, he joined the School of Electrical Electronic and Computer Engineering, University of Western Australia, where he is currently a Professor. His research interests include power systems, renewable energy, functional observers, state estimation, and biomedical engineering.

Dr. Fernando has served as an Associate Editor for the IEEE TRANSACTIONS ON INFORMATION TECHNOLOGY IN BIOMEDICINE and also as a Guest Editor for the *Journal of Optimal Control Applications and Methods.* He is currently an Associate Editor for the IEEE TRANSACTIONS ON CIRCUITS AND SYSTEMS–II and IEEE ACCESS.

Tat Kei Chau (S'16) received the B.Eng. (Hons.) degree in electronic and communication engineering with first-class honors from the City University of Hong Kong, Hong Kong, in 2010, and the Master's degree in electrical and electronic engineering with Distinction from the University of Western Australia, Crawley, WA, Australia, in 2014, where he is currently working toward the Ph.D. degree. His research interests are in power electronics, power system analysis and control, microgrids, smart grids, renewable energy integration, load and power generation forecasting, and dynamic state estimation.

Herbert Ho-Ching Iu (S'98–M'00–SM'06) received the B.Eng. (Hons.) degree in electrical and electronic engineering from the University of Hong Kong, Hong Kong, in 1997. He received the Ph.D. degree from the Hong Kong Polytechnic University, Hong Kong, in 2000. In 2002, he joined the School of Electrical, Electronic and Computer Engineering, University of Western Australia where he is currently a Professor. His research interests include power electronics, renewable energy, nonlinear dynamics, current sensing techniques, and memristive systems.

Dr. Iu currently serves as a Guest Editor for the IEEE TRANSACTIONS ON INDUSTRIAL ELECTRONICS, leading Guest Editor in Chief of the IEEE TRANSACTIONS ON EMERGING AND SELECTED TOPICS IN CIRCUIT AND SYSTEMS Special Issue on "Complex Networks for Modern Smart Grid Applications" and several other journals including *IET Power Electronics*.